



**Integrated hydrological modeling of the North China Plain**

H. Qin et al.

This discussion paper is/has been under review for the journal Hydrology and Earth System Sciences (HESS). Please refer to the corresponding final paper in HESS if available.

# Integrated hydrological modeling of the North China Plain and implications for sustainable water management

H. Qin<sup>1</sup>, G. Cao<sup>1</sup>, M. Kristensen<sup>2</sup>, J. C. Refsgaard<sup>3</sup>, M. O. Rasmussen<sup>4</sup>, X. He<sup>3</sup>, J. Liu<sup>1</sup>, and C. Zheng<sup>1,5</sup>

<sup>1</sup>Center for Water Research, College of Engineering, Peking University, Beijing, 100871, China

<sup>2</sup>ALECTIA, Teknikerbyen 34, 2830 Virum, Denmark

<sup>3</sup>Geological Survey of Denmark and Greenland (GEUS), 1350 Copenhagen, Denmark

<sup>4</sup>GRAS A/S, Oester Voldgade 10, 1350 Copenhagen, Denmark

<sup>5</sup>Department of Geological Sciences, University of Alabama, Tuscaloosa, AL 35487, USA

Received: 31 January 2013 – Accepted: 8 March 2013 – Published: 19 March 2013

Correspondence to: C. Zheng (czheng@ua.edu)

Published by Copernicus Publications on behalf of the European Geosciences Union.

Title Page

Abstract

Introduction

Conclusions

References

Tables

Figures



Back

Close

Full Screen / Esc

Printer-friendly Version

Interactive Discussion



## Abstract

Groundwater overdraft has caused fast water level decline in the North China Plain (NCP) since the 1980s. Although many hydrological models have been developed for the NCP in the past few decades, most of them deal only with the groundwater component or only at local scales. In the present study, a coupled surface water–groundwater model using the MIKE SHE code has been developed for the entire alluvial plain of the NCP. All the major processes in the land phase of the hydrological cycle are considered in the integrated modeling approach. The most important parameters of the model are first identified by a sensitivity analysis and then calibrated for the period 2000–2005. The calibrated model is validated for the period 2006–2008 against daily observations of groundwater heads. The simulation results compare well with the observations where acceptable values of root mean square error (RMSE) and correlation coefficient ( $R$ ) are obtained. The simulated evapotranspiration (ET) is then compared with the remote sensing (RS) based ET data to further validate the model simulation. The comparison result with a  $R^2$  value of 0.93 between the monthly averaged values of simulated actual evapotranspiration (AET) and RS AET for the entire plain shows a good performance of the model. The water balance results indicate that more than 69 % of water leaving the flow system is attributed to the ET component. Sustainable water management analysis of the NCP is conducted using the simulation results obtained from the integrated model. An effective approach to improve water use efficiency in the NCP is by reducing the actual evapotranspiration, and that water-saving technologies based on this approach, such as change of crop rotation types, may be adopted.

## 1 Introduction

The use of groundwater as a resource for water supply to urban areas and for irrigation has increased dramatically during the past decades, while in many areas of the world there is still a large unused potential for increased groundwater exploitation

**HESSD**

10, 3693–3741, 2013

## Integrated hydrological modeling of the North China Plain

H. Qin et al.

Title Page

Abstract

Introduction

Conclusions

References

Tables

Figures

⏪

⏩

◀

▶

Back

Close

Full Screen / Esc

Printer-friendly Version

Interactive Discussion





**Integrated hydrological modeling of the North China Plain**

H. Qin et al.

[Title Page](#)[Abstract](#)[Introduction](#)[Conclusions](#)[References](#)[Tables](#)[Figures](#)[⏪](#)[⏩](#)[◀](#)[▶](#)[Back](#)[Close](#)[Full Screen / Esc](#)[Printer-friendly Version](#)[Interactive Discussion](#)

a fixed fraction of the precipitation without considering dynamics of the evaporation or the existence of irrigation. Kendy et al. (2003) pointed out that the recharge fraction depends on the quantity and temporal distribution of precipitation and irrigation. The simplified treatment of recharge introduces uncertainty in evaluating the groundwater recharge and hence in closing the water balance. The Institute of Remote Sensing Applications (IRSA), Chinese Academy of Sciences recently provides estimates of evapotranspiration over the NCP using a combination of data from flux stations and remote sensing data (Wu et al., 2012). In order to make full use of such evapotranspiration data and hence make a more reliable assessment of the water balance for the NCP aquifer, it is required to use an integrated hydrological model with a coupled groundwater-surface water approach (Henriksen et al., 2003; Doummar et al., 2012; Li et al., 2012; Stisen et al., 2012). In the present study, the recharge component is treated as a seasonal variable and is distributed based on the formulations of evapotranspiration and unsaturated flow. Precipitation, irrigation, potential evapotranspiration, and crop and soil properties are also considered in the model to calculate the recharge.

The objectives of the present study are to develop an integrated hydrological model for the NCP aquifer system using the MIKE SHE modeling tool and to analyze and understand the water balance components of the NCP. The model is used to assess the potential of using the RS based evapotranspiration in order to improve the water balance calculations and to discuss the perspectives of using an integrated hydrological model to support sustainable water resources management in the NCP.

## 2 Study area and data

### 2.1 The North China Plain

Geographically, the North China Plain (NCP) refers to the alluvial plain north of the Yellow River, south of the Yanshan Mountain and east of the Taihang Mountain. Figure 1 shows the region of the NCP, spanning from 32° N to 40° N and from 114° E to 121° E. It

**Integrated hydrological modeling of the North China Plain**

H. Qin et al.

[Title Page](#)[Abstract](#)[Introduction](#)[Conclusions](#)[References](#)[Tables](#)[Figures](#)[⏪](#)[⏩](#)[◀](#)[▶](#)[Back](#)[Close](#)[Full Screen / Esc](#)[Printer-friendly Version](#)[Interactive Discussion](#)

includes all part of Beijing and Tianjin Municipality, most part of Hebei Province and the northern part of the Yellow River Basin of Shandong Province and Henan Province. The total area of the NCP is 140 000 km<sup>2</sup> and it is one of the most densely populated regions in the world, with an average population density of approximately 800 persons km<sup>-2</sup>. In the year 2000, the total population of the NCP was around 130 million. It is the center of China's political, economic and cultural development. Due to its sub-humid to semi-arid climate condition, the NCP is very prone to drought, which stresses sustainable water resources management of that region (Liu et al., 2008; Zheng et al., 2010; Qin et al., 2012).

The NCP aquifer is divided into four main hydrogeological zones from the Taihang Mountains on the west to the Bohai Sea on the east; these zones are based on the geomorphology of Paleochannels. According to their sedimentary character and relative geographic positions, the region consists of a piedmont plain, an alluvial fan, an alluvial plain, and a coastal plain (Wu et al., 1996; Cao et al., 2013).

The climate in the NCP is continental semi-arid, with average annual temperature of 12–13 °C. The mean annual precipitation of 1951–1995 is 554 mm, while the seasonal distribution of precipitation is uneven, with about 75 % of its precipitation occurring throughout the summer flood season from July to August (Qin et al., 2012). This climate type is the reason of the frequent flooding and drought events in the NCP region. There have been 135 flooding years and 140 drought years in the NCP in the last 500 yr (Huai River Commission, 1998). The water resources per capita in the NCP is 501 m<sup>3</sup>, which is only 23 % of the China's average (Xia et al., 2007). Groundwater has become an indispensable factor to support the economic and social sustainable development of the NCP. Currently, the groundwater resources have accounted for more than 70 % of the total water supply in Beijing, Shijiazhuang and many other cities in the NCP. Overexploitation of the groundwater resources is very common, especially during the past few decades, where the acceleration of industrialization in China took place. Moreover, the industrialization and growth of the population are unsustainable and the economic development in the area is likely to be limited due to the scarcity of

water in near future (Qin et al., 2012). Agriculture accounts for 85 % of the total water consumption in the NCP (Xu et al., 2005). Winter wheat and summer maize are the main crops in the NCP rotation system, accounting for about 80 % of total cultivated area and 90 % of grain yield in the NCP (China Statistical Yearbook, 2010; Shu, 2010).

Table 1 lists the types and sources of the data used in the NCP model setup. Data defining the driving forces for the water flow is described in the following sections.

## 2.2 Climate data

In the NCP model, climate data include precipitation rate and reference evapotranspiration. The spatial distribution type of precipitation rate is fully distributed, whereas that of the reference evapotranspiration is station based. The precipitation data are collected from Tropical Rainfall Measuring Mission (TRMM) of NASA Science (<http://trmm.gsfc.nasa.gov>) with a resolution of 25 km for the simulation period 2000–2008 on a daily basis. The precipitation data are resampled to 10 km resolution and re-projected to the model grid. The data of reference evapotranspiration are generated using data from 22 meteorological stations (locations are shown in Fig. 1) provided by Chinese Meteorological Data Service (CMDS). The station based evapotranspiration data are distributed using Thiessen Polygons. Table 2 lists the information of the meteorological stations, including station name, elevation, latitude, longitude and which municipality or province this station belongs to.

## 2.3 Land use data

The land use map listed as Fig. 2a is created from MODIS NDVI products from 2003. The classification is made from the seasonal variation in NDVI using the method proposed by Kang et al. (2007) (Shu, 2010). It is assumed that the generated land cover classification can represent the conditions throughout the whole simulation period. The land cover classification is divided into nine classes: water, resident, wheat and corn 10, rock, fruit tree, cotton 20, cotton 30, wheat and corn 20, and wheat and corn 30,

Title Page

Abstract

Introduction

Conclusions

References

Tables

Figures

⏪

⏩

◀

▶

Back

Close

Full Screen / Esc

Printer-friendly Version

Interactive Discussion

## Integrated hydrological modeling of the North China Plain

H. Qin et al.

Title Page

Abstract

Introduction

Conclusions

References

Tables

Figures



Back

Close

Full Screen / Esc

Printer-friendly Version

Interactive Discussion

where “10” refers to piedmont district, while “20” and “30” refer to the central and coastal plains, respectively. The land use type wheat and corn is divided into three types while the type cotton is divided into two types. One reason for doing so is that the vegetation parameters (e.g. leaf area index, crop coefficient and root depth) are different in piedmont plain, alluvial plain and coastal plain (Giovanni et al., 2009a,b). Another reason is that even the same crop needs different amount of irrigation water for different plains in the NCP (Ma et al., 2011). The vegetation parameters are measured on the basis of experience or collected from literature. In this study, the leaf area index (LAI) and root depth take the same values for a certain vegetation type, while crop coefficient ( $K_c$ ) and irrigation water requirement have different values for the same vegetation type. These are required input data for the model setups and Table 3 lists the typical value ranges of LAI, root depth and  $K_c$  for each crop in the NCP.

The typical crop rotation in the NCP is winter wheat and summer corn. The growth of winter wheat is described by six stages from October to early June (approximately 210 days): sowing, wintering, revival, jointing, flowering, and grain filling. And from June to September the summer corn is grown described by four stages: sowing, emergence, jointing-flowering, and grain filling (Shu, 2010). The growing season of cotton and fruit trees is the same, which is from May to October. Irrigation is applied according to the growing stages of different crops. The irrigation frequency and yearly irrigation water amount for these crops are listed in Table 3.

### 2.4 Pumping data

Irrigation is estimated according to different crop types. Different irrigation frequency and water amount are applied to different crops. Take winter wheat for instance; there are five irrigation times in one year and each time winter wheat is irrigated with a certain amount of water. The yearly irrigation water of winter wheat can be computed by multiplying the irrigation frequency and irrigation water needed each time. Then the total irrigation water is the sum of water amounts of all the crops in this area.

## Integrated hydrological modeling of the North China Plain

H. Qin et al.

Title Page

Abstract

Introduction

Conclusions

References

Tables

Figures

⏪

⏩

◀

▶

Back

Close

Full Screen / Esc

Printer-friendly Version

Interactive Discussion

Most of the water supply to the cities in the NCP is abstracted from groundwater including both the shallow and deep aquifer systems. We consider groundwater abstraction for domestic and industrial use in all the 21 cities (Beijing, Tianjin, Qinhuangdao, Tangshan, Shijiazhuang, Handan, Xingtai, Baoding, Langfang, Cangzhou, Hengshui, Jinan, Dongying, Binzhou, Dezhou, Liaocheng, Anyang, Hebi, Xinxiang, Jiaozuo and Puyang) in the entire NCP aquifer (Qin et al., 2012). Abstraction data of these cities are provided by Qin et al. (2012) and the pumping wells are assumed to pump water from the upper and middle parts of the groundwater zone.

The groundwater pumping for domestic and industrial use is formulated based on the hypotheses from Qin et al. (2012): (1) collect time series data of total domestic water demand  $DWT(i, t)$  and total industrial water demand  $IWT(i, t)$  of the  $i$ -th city, respectively, where  $1 \leq i \leq 21$ , and  $t$  is the simulation time. The total domestic and industrial water demands are estimated based on the population and industrial output using the System Dynamics method (Qin et al., 2012). (2) Randomly generate  $N_i$  points in the  $i$ -th city area, respectively, where  $1 \leq i \leq 21$  and  $10 \leq N_i \leq 20$ . The random point's number of each city depends on the ranking of relative importance of that city. For example, there are 20 points in Beijing City while 10 points in Jiaozuo City. Each random point is assumed as a pumping well in that area and the same pumping rate is applied on each well. (3) For the  $i$ -th city, calculate the pumping rate for each well by Eq. (1):

$$DW(i, t) = \frac{DWT(i, t)}{N_i} \quad IW(i, t) = \frac{IWT(i, t)}{N_i} \quad 1 \leq i \leq 21 \quad (1)$$

where  $DW(i, t)$  and  $IW(i, t)$  are domestic and industrial water demand pumping rate for each well in the  $i$ -th city. A total of 580 pumping wells are generated and distributed in the NCP aquifer after these three steps.

## 2.5 ETWatch data

ETWatch has originally been developed as an operational software system for regional ET monitoring, on request of the Hai Basin commission (Wu et al., 2008a; Xiong et al.,

**Integrated  
hydrological  
modeling of the  
North China Plain**

H. Qin et al.

[Title Page](#)[Abstract](#)[Introduction](#)[Conclusions](#)[References](#)[Tables](#)[Figures](#)[⏪](#)[⏩](#)[◀](#)[▶](#)[Back](#)[Close](#)[Full Screen / Esc](#)[Printer-friendly Version](#)[Interactive Discussion](#)

2010a,b). ETWatch is an integration of the “Residue Approach” and Penman–Monteith (P–M) (Wu et al., 2011a,b, 2012). It is an operational processing chain starting from data pre-processing to application products, utilizing spatial information of climate, soil type, land use, vegetation cover, digital elevation and remote sensed land surface parameters. The surface energy balance algorithm for land (SEBAL) and the surface energy system (SEBS) are integrated into ETWatch to estimate surface fluxes on clear-sky condition, while the Penman-Monteith is applied to retrieve daily ET based on the surface resistance model, the meteorological data and the surface parameters from remote sensing (Wu et al., 2008b). The ETWatch data is provided by IRSA of Chinese Academy of Sciences and used in the ET comparison part of our study to validate the model simulation (Wu et al., 2012).

### 3 Model setup and calibration

#### 3.1 Modeling tool

15 The modeling tool used in this study, MIKE SHE, is developed by DHI (<http://www.dhigroup.com>). It was originally developed as the SHE (Système Hydrologique Européen) model (Abbott et al., 1986a,b) along with the British Institute of Hydrology and SOGREAH (France). MIKE SHE is a deterministic, distributed, physically based hydrologic modeling system that covers the major processes in the hydrologic cycle and includes process models for evapotranspiration, overland flow, channel flow, unsaturated flow, groundwater flow, and their interactions. A finite difference approach is used to solve the partial differential equations describing the processes of overland (two-dimensional Saint-Venant equation), channel (Kinematic Routing solver), unsaturated (2-layer water balance method) and saturated subsurface flows (three dimensional Boussinesq equation) whereas analytical solutions are used for describing inter-  
20 ception and evapotranspiration (Refsgaard and Storm, 1995). Since the precipitation is limited in winter, snow melt is not activated in the NCP model. Other major components

included to describe the hydrological system are the irrigation and the groundwater pumping.

### 3.2 Model discretization

The integrated MIKE SHE model of NCP covers the period from 1 January 2000 to 31 August 2008, a total of nearly nine years. Due to the different time scales in different flow systems, the time step of groundwater flow is one day while that of the river flow is five minutes. The grid covering the modeling area is discretized to 300 columns and 350 rows with a uniform cell size of 2 km × 2 km, a total simulation area of 140 000 km<sup>2</sup>. The model grid is discretized into three computational layers for the unsaturated zone (Cao et al., 2013). The hydrogeological zone is divided to four layer/zones and the first computational layer includes the first two hydrogeological zones, the second computational layer is the third hydrogeological zone and the third computational layer is the fourth hydrogeological zone. The Shuttle Radar Topography Mission (SRTM) (Rabus et al., 2003) elevation data at 90 m resolution has been aggregated to the model grid and used as the top elevation (Cao et al., 2013).

### 3.3 Rivers and lakes

There are many rivers in the entire NCP area and the five major rivers – Luan River, Yongding River, Hutuo River, Zhang River and Wei River – are considered in NCP model (Fig. 3). These rivers are selected due to data availability and the fact that the unconsidered rivers in the NCP have run dry after the year 2000, which is the start year of the simulation period. A simulation time step of 5 min is used in the MIKE 11 river model. The network, cross-section and boundary of the rivers are input data of this section. These data are provided by China Institute of Water Resources and Hydropower Research (IWHR). The geometry of each river branch is specified in terms of cross sections. Cross sections and datum are important to both conveyance capacity and storage capacity at different reaches of river system. Two types of river boundaries

## Integrated hydrological modeling of the North China Plain

H. Qin et al.

[Title Page](#)

[Abstract](#)

[Introduction](#)

[Conclusions](#)

[References](#)

[Tables](#)

[Figures](#)

[⏪](#)

[⏩](#)

[◀](#)

[▶](#)

[Back](#)

[Close](#)

[Full Screen / Esc](#)

[Printer-friendly Version](#)

[Interactive Discussion](#)



are considered for each river branch in the study: inflow at the upstream and water level at the downstream. These two boundaries are constant ones due to the data availability of the rivers. Each river exchanges water with groundwater zone through the coupling reaches. Each coupling reach is interpolated to a MIKE SHE river link, which is located at the nearest boundary between grid cells (DHI, 2008a).

### 3.4 Unsaturated zone

Soil types and their related properties are very important for the unsaturated flow. Figure 2b is the soil type map of the NCP, with loam as the dominant type and silty loam and sand as secondary types. Sandy soil is mainly located along Hutuo River and at other isolated patches within the model area. Other sediment type like silt loam is only found at few locations (Shu, 2010). The 2-layer Water Balance Model for the unsaturated zone requires the following data of each soil type: water content at saturation ( $\theta_{\text{sat}}$ ), water content at field capacity ( $\theta_{\text{fc}}$ ), water content at wilting point ( $\theta_{\text{wp}}$ ) and saturated hydraulic conductivity ( $K_s$ ). The values of these parameters of the three soil types are listed in Table 4. Additional parameters are required for MIKE SHE to calculate the actual evapotranspiration (ET). The ET surface depth, which equals the thickness of the capillary zone, is required. Over the ET surface depth the ET is reduced linearly (DHI, 2008a). The value of the ET surface depth is set to 0.2 m in the NCP model to represent the loamy and sandy soil types.

### 3.5 Saturated zone

The groundwater zone is conceptualized into three computational layers describing a multi-layer, heterogeneous and anisotropic 3-D hydrogeological model of the NCP aquifers. The layers extend to a depth of more than 500 m below the land surface. The hydrogeological conceptualization proposed by Cao et al. (2013) is adopted in our study and the hydrogeological parameters are distributed in the layers of the entire NCP. The hydrogeological model is specified via hydrogeological units which are

Title Page

Abstract

Introduction

Conclusions

References

Tables

Figures

⏪

⏩

◀

▶

Back

Close

Full Screen / Esc

Printer-friendly Version

Interactive Discussion

## Integrated hydrological modeling of the North China Plain

H. Qin et al.

Title Page

Abstract

Introduction

Conclusions

References

Tables

Figures

⏪

⏩

◀

▶

Back

Close

Full Screen / Esc

Printer-friendly Version

Interactive Discussion

distributed to cover the different layers. For each hydrogeological unit the associated hydrogeological properties are specified separately. The aquifer is discretized using 27 hydrogeological units (Fig. 2c and d) for the reasons that it represents the geological and hydrogeological characteristics of the NCP aquifer. Since the geological units adopted from Cao et al. (2013) represent categorized zonal index using a continuous K field, they do not have hydrogeological meanings. The same parameters (horizontal conductivity  $K_{xx}$  and  $K_{yy}$ , vertical conductivity  $K_{zz}$ , specific yield  $S_y$ , and storage coefficient  $S_s$ ) are used in the same unit. Layer 1 is shallow aquifer zone while layer 2 and 3 are deep aquifer zone. As suggested by Cao et al. (2013), layer 2 and 3 are described by the same distribution of hydrogeological units (Fig. 2d).

Initial potential heads of 1 January 2000 for layer 1, 2 and 3, which are used as the initial conditions in the model simulation, are adopted from Cao et al. (2013). Three types of boundary conditions are assigned to layer 1: fixed head to zero, fixed head to initial value and zero-flux. The first one is used at the northeastern part of the model, where the land intercepts with the Bohai Gulf, to represent the average sea level. The second one is used at the south and southeastern parts of the model where it is bounded by the Yellow River. The last one is used to the western boundary, which is the interface between the Taihang Mountain and the piedmont plain. For layer 2, two boundary conditions are used: the northeastern part, which is the interface with the Bohai Gulf, is assigned by a zero head condition; the rest of the area is assigned by a zero-flux condition. While for the third layer, a zero-flux condition is applied for the whole boundary.

### 3.6 Model calibration

The primarily aim of the calibration process is to obtain a set of model parameters that provide a satisfactory agreement between simulation results and field observations. The NCP model is calibrated using AutoCAL as an optimization tool, which is included in MIKE SHE software package (Madsen, 2003). The calibration targets are groundwater heads, which are very important in the model simulation and will influence saturated

zone flow and actual ET. There are 226 observation wells (locations are shown in Fig. 1) distributed in the study area that are used in the calibration procedure. Calibration results of 9 selected observation wells (shown as selected wells with names in Fig. 1) are presented in this study. The criteria for the selection of these nine observation wells are that they need to have complete time series for the entire model simulation period and they are less disturbed by the local pumping activities. Table 5 lists the information of these selected observation wells. The information presented here includes the geographical locations and the screen depth where the groundwater head is measured. The simulation period is divided into two stages: the calibration stage from 2000 to 2005 and the validation stage from 2006 to 2008.

The root mean square error (RMSE), which is an aggregated measure that includes both the bias and the dynamical correspondence (Anderson and Woessner, 1992) and can be calculated by Eq. (2), is the objective function minimized in the auto-calibration process of the NCP model. Furthermore, there are another five quantitative performance criteria as defined in Eqs. (3) to (7): ME (mean error), MAE (mean absolute error),  $STD_{res}$  (standard deviation of residuals),  $R$  (coefficient of correlation), and  $E$  (Nash–Sutcliffe model efficiency coefficient) (Nash and Sutcliffe, 1970).

$$RMSE = \sqrt{\frac{1}{N} \sum_{i=1}^N (O_i - S_i)^2} \quad (2)$$

$$ME = \frac{1}{N} \sum_{i=1}^N (O_i - S_i) \quad (3)$$

$$MAE = \frac{1}{N} \sum_{i=1}^N |O_i - S_i| \quad (4)$$

**Integrated hydrological modeling of the North China Plain**

H. Qin et al.

Title Page

Abstract

Introduction

Conclusions

References

Tables

Figures

⏪

⏩

◀

▶

Back

Close

Full Screen / Esc

Printer-friendly Version

Interactive Discussion



$$\text{STD}_{\text{res}} = \sqrt{\frac{1}{N} \sum_{i=1}^N (O_i - S_i - \text{ME})^2} \quad (5)$$

$$R = \frac{\sum_{i=1}^N (O_i - \bar{O})(S_i - \bar{S})}{\sqrt{\sum_{i=1}^N (O_i - \bar{O})^2} \sqrt{\sum_{i=1}^N (S_i - \bar{S})^2}} \quad (6)$$

$$E = 1 - \frac{\sum_{i=1}^N (O_i - S_i)^2}{\sum_{i=1}^N (O_i - \bar{O})^2} \quad (7)$$

where  $O_i$  is the  $i$ -th ( $i$  is the daily index) observed value,  $S_i$  is the  $i$ -th simulated value,  $\bar{O}$  is the average observed value,  $\bar{S}$  is the average simulated value,  $N$  is the total number of corresponding measurements and simulations.

AutoCAL applies the shuffled complex evolution (SCE) optimization algorithm, which is a global optimization algorithm that combines various search strategies, including (i) competitive evolution, (ii) controlled random search, (iii) the simplex method, and (iv) complex shuffling (Madsen, 2003).

## 4 Results and discussion

### 4.1 Calibration and validation results

Prior to the calibration, a sensitivity analysis, is performed to identify the most sensitive parameters of the NCP model. The parameters related to the unsaturated zone are adopted from Shu (2010) and thus are not included in the calibration procedure. The parameters selected as the most sensitive parameters and then used in the calibration stage are listed in Table 6. The final values of the parameters, which are suggested as the optimal parameters after the calibration, are also listed in Table 6. The most sensitive parameters are horizontal conductivities and specific yield for geological units.

The horizontal conductivities are log-transformed in the optimization process. To keep the number of free parameters as low as possible, some parameters are tied to each other (Table 6). The calibration performance criteria calculated of each observation well for the calibration period and validation period are listed in Table 7. At the calibration stage, the performance criteria suggest reasonable calibration results for the model. For most observation wells, the correlation coefficient is above 0.7, which indicates good agreement between the observed and the simulated groundwater head. The values of RMSE of most wells are between 0.5 and 2.5 m, which are considered small for a large simulation area. The deficiencies of RMSE, ME and MAE are likely to be caused by the aggregation and simplification of parameters for the groundwater flow system. At the validation stage, except for wells #113 and #116, the correlation coefficient for most wells are very high, which shows that the calibration is rather successful. The performance result for the total 226 wells is also listed in Table 7. The  $R$  value is 0.850 while the ME, MAE and RMSE values are 3.4, 9.9 and 12.6 m, respectively. These values are considered small relatively to the maximum groundwater level variations of about 60 and 70 m in the shallow and deep aquifer zones, respectively (Cao et al., 2013). Overall the results of the model calibration basically confirm the validity of the NCP model.

Figure 4 lists the comparison of simulated and observed groundwater heads of selected observation wells distributed in the NCP for the calibration period and validation period. The simulated groundwater dynamics fits well with the observations during both periods. A decline trend is observed in all the simulated and observation wells. For a number of wells, the shapes of the simulated heads are lack of temporal variation. This phenomenon may be explained by the depth of the wells and the influence of local pumping activities. As seen in Table 5, wells #6, #66, #123 and #140 happen to be deep drilling wells; therefore the temporal variation from the groundwater recharge has little or no effect at that depth. Another possible reason is that intensive pumping activities that take place at the same model grid as the pumping well may have a smoothening effect on the shape of the simulated head curve. In wells #6, #66 and

# HESSD

10, 3693–3741, 2013

## Integrated hydrological modeling of the North China Plain

H. Qin et al.

Title Page

Abstract

Introduction

Conclusions

References

Tables

Figures

⏪

⏩

◀

▶

Back

Close

Full Screen / Esc

Printer-friendly Version

Interactive Discussion



**Integrated  
hydrological  
modeling of the  
North China Plain**

H. Qin et al.

Title Page

Abstract

Introduction

Conclusions

References

Tables

Figures

⏪

⏩

◀

▶

Back

Close

Full Screen / Esc

Printer-friendly Version

Interactive Discussion

#116, the simulated curve and the observed curve are in close agreement, which are reflected by the high correlation coefficient and the model efficiency values. The correlation coefficients of them are 0.911, 0.899 and 0.846 for the calibration period. Due to the data availability, the time series of observed heads are a little shorter than that of the simulated heads in some wells. However, the performance in general between the simulated heads and the observed heads is not affected by this factor. The validation results in Fig. 4 further support the reliability of the calibrated hydrological model of the NCP. Figure 5 lists the comparison between the observed and simulated groundwater heads for the total 226 wells. This comparison figure is also a support of the hydrological model's reliability from a general performance perspective of all observation wells used in the calibration and validation processes.

## 4.2 Comparison of actual evapotranspiration

For comparison with the model results, estimates of actual evapotranspiration (AET) are obtained based on remote sensing data provided by IRSA (Wu et al., 2011a,b). Daily estimates of AET are produced based on data from the MODIS satellites at a spatial resolution of 1 km, combined with interpolated data from standard meteorological stations within and adjacent to the NCP (referred to as ETWatch in the following). The ETWatch data are available for the period January 2002 to August 2008.

Figure 6 shows a comparison of the monthly AET averaged over entire model domain, excluding an area to the south-east where the ETWatch data are not available. Our model offers a good description of the seasonal dynamics of AET, as reflected in Fig. 6, including the double peak for each year. The double peak is determined by the winter wheat and summer corn rotation type of the NCP agriculture. The model simulated AET fits very well with the remote sensing based AET, with a  $R^2$  value equal to 0.93, RMSE value equal to 10.4 mm/month and MAE value equal to 8.3 mm/month. The model simulated ET-values tend to be underestimated compared to the ET-Watch estimates especially for higher values.

**Integrated  
hydrological  
modeling of the  
North China Plain**

H. Qin et al.

[Title Page](#)[Abstract](#)[Introduction](#)[Conclusions](#)[References](#)[Tables](#)[Figures](#)[⏪](#)[⏩](#)[◀](#)[▶](#)[Back](#)[Close](#)[Full Screen / Esc](#)[Printer-friendly Version](#)[Interactive Discussion](#)

However, the simulated mean monthly AET are not always in good agreement with the ETWatch values when considering the spatial distribution across the NCP, especially during the period with high AET. The discrepancy is not surprising due to the very different parameterizations of ET in the two methods. Figure 7 shows an example of the yearly aggregated AET values for the two methods for 2002. Many spatial features can be found in both estimates of AET, but there are also significant differences. For the model simulated values, the northern part of the model domain lacks some information on the land cover, causing the model to overestimate the AET rates for urban areas such as the Beijing area. Another notable difference is the occurrence of an area with very high AET-values along the coastline in the ETWatch product. This is not the case for the model simulations where this area is dominated by low AET-values.

The spatial patterns of AET stratified by the land cover information used in the model are analysed (described in Sect. 2.3). Eight classes (the class type Rock is ignored because it has no data and no effect on the model) are considered to represent different land covers (e.g. agricultural areas and urban areas), as well as different irrigation schemes applied in different regions (e.g. there are several cotton classes – see Fig. 3a). Overall, most classes performe similar to what is shown in Fig. 6, with linear regressions of  $R^2$  values  $> 0.92$  and slopes around 0.85. The main difference between the simulated AET-values and the ETWatch estimates is that they show different spatial patterns in each land use class. For ETWatch, there are much larger differences between the different land cover classes than the case for the model simulated values. As no independent validation data available, it is yet not possible to further evaluate the results of the two ET products, but it is clear that the model simulated ET has more homogenous fields compared to that of the ETWatch. Figure 8 shows the mean annual AET for the two different methods. We have also added the variance in terms of the standard deviation, calculated based on the average values for each of the eight classes considered. For all years except 2006, the standard deviation is higher for the ETWatch data than for the model estimates.

It is without doubt that the two approaches in estimating AET are fundamentally different. However, the AET comparison indicates that to some extent the vegetation parameters of our model are reasonable since the magnitude and timing between the two AET estimates are comparable based on the monthly data. As AET is a very important component in NCP's water balance analysis, this comparison of AET is a useful test of the NCP model.

### 4.3 Surface water discharge results

Simulated surface water discharge at three locations of two river channels within the MIKE 11 river model are shown in Fig. 9a and b. The discharges of the rivers are decreasing during the simulation period, which is reasonable since most of the rivers in the NCP have run dry in recent years. The stream-flows under all circumstances are small compared to AET. Due to the lack of time series observations, quantitative comparison between simulated and observed stream flows is not presented. However it could bring new insights to the model calibration using stream flow data in future, when the observed stream flow data become available.

### 4.4 Water balance analysis

Water balance is an important and essential result of the model simulation, which gives us helpful information on available water resources supply and demand in that study area. Water balance analysis is a useful tool in the process of the NCP's sustainable water management. Figure 10 shows the yearly averaged water balance of the entire NCP aquifer system for the whole simulation period while Table 8 shows the annual water balance components for the simulation period. The main components included in the total water balance of the NCP model are precipitation, irrigation, evapotranspiration, and pumping, where the first two are water inflow of the groundwater zone and the latter two are water outflow of the groundwater zone. In general, the total inflow in one year is 825.1 mm while the total outflow in one year is 824.8 mm, with a total

[Title Page](#)

[Abstract](#)

[Introduction](#)

[Conclusions](#)

[References](#)

[Tables](#)

[Figures](#)

[⏪](#)

[⏩](#)

[◀](#)

[▶](#)

[Back](#)

[Close](#)

[Full Screen / Esc](#)

[Printer-friendly Version](#)

[Interactive Discussion](#)



---

**Integrated  
hydrological  
modeling of the  
North China Plain**H. Qin et al.

---

[Title Page](#)[Abstract](#)[Introduction](#)[Conclusions](#)[References](#)[Tables](#)[Figures](#)[⏪](#)[⏩](#)[◀](#)[▶](#)[Back](#)[Close](#)[Full Screen / Esc](#)[Printer-friendly Version](#)[Interactive Discussion](#)

error of  $-0.3$  mm (Fig. 10). Most of the water (69 %) entering the model area leaves the hydrological system through evapotranspiration, and 30 % leaves the system through pumping. This shows an obvious deficit in the total water balance and Fig. 10 shows that the total water going out of the system is more than that entering the system.

5 Except for some wet years, such as 2003, 2004 and 2008, Table 8 shows that the actual ET is higher than the precipitation, which indicates an unsustainable use of the water resources in the NCP. Therefore it is an effective way to improve water use efficiency and water sustainable management by reducing the actual evapotranspiration of the NCP as it controls most water out of the aquifer system. Furthermore, the total  
10 evapotranspiration is larger than the total precipitation for the entire simulation period, a corresponding result of which is the decline of saturated zone and unsaturated zone storage. The total decline in the saturated zone and unsaturated zone storage during the entire simulation period are 519 and 68 mm, respectively. A declining trend of the storage indicates an unsustainable groundwater exploration in the study area (Fig. 11).  
15 The groundwater storage change follows an annual cycle, which is decrease in dry winter and increase in wet summer. As noticed in Table 8, the values of UZ storage change in 2003, 2007 and 2008 and SZ storage change in 2003 are positive, which indicates a rise in storage. It is due to the high precipitation in these years. The high annual precipitation in 2003 causes an overall increased groundwater storage and Fig. 4 witnesses an associated rising in groundwater table. Compared with other components, the base flow from and to the rivers are very small, which indicates that the inflow from the rivers is less important for the overall water balance of the NCP aquifer system.

The results of the water balance analysis have significant implications for the sustainable water management in the NCP. Evapotranspiration is the only actually water  
25 consumed or depleted of the hydrologic system (Kendy, 2007). Based on this fact, it is an effective and practical way to reduce evapotranspiration to release the water shortage pressure in the NCP area, as about 69 % of the water in the NCP leaves the system by the way of ET. Water-saving technologies based on this idea can be adopted to reduce evaporation. And we can change the crop rotation type to help reducing the ET.

For example, the crop rotation type with less evaporation is a good choice to replace the existing one.

Intensive pumping activities have always been blamed to be the main reason for the groundwater depletion in the NCP. They are also held responsible for the problems in the NCP's sustainable water management process. Table 8 and Fig. 10 show that the pumping water takes up about 33 % of the precipitation and irrigation water in the NCP. Therefore, the current pumping capacity is not sustainable from the aspect of the total water balance analysis. Nevertheless, the unreasonable and extensive distribution of the pumping activities in the NCP can hardly absolve itself from the blame. The actual pumping taking place is very uncertain and it needs to be addressed to get more valid model, which can be used to investigate different water management approaches in the NCP area. It is not too much of this blame once people in the NCP do not take a sustainable distribution of the pumping activities. Amongst the information which could help improve the model, it is the one on pumping rate and location of well fields that are the two most important factors that needed to be controlled and optimized for the entire NCP. Besides, different irrigation schemes could also help improve the consumption of water in the NCP area.

Figure 12 shows (1) the initial head distribution (1 January 2000) for layer 1, 2 and 3, respectively; (2) the simulated head distribution at the end of the simulation period (31 August 2008) for layer 1, 2 and 3, respectively. For the shallow geological layer (layer 1 in this study area, Fig. 12a, b), the depression cone near the city Shijiazhuang, which is the capital of Hebei province, has already existed in 2000 and extended further in the next simulation period. While for the deep geological layers (layer 2 and 3, Fig. 12c–f), along with the development of economic and social in the NCP, more and more groundwater is pumping from these two layers, which is used to meet the needs of the irrigation and the industrial and agricultural production. As discussed above, irrigation is the biggest consumer of groundwater in the NCP, which is the major reason for the groundwater level decline in this area. The groundwater levels have declined about 20 to 30 m in the plain area during the simulation period from 2000 to 2008. The water

## HESSD

10, 3693–3741, 2013

### Integrated hydrological modeling of the North China Plain

H. Qin et al.

Title Page

Abstract

Introduction

Conclusions

References

Tables

Figures

⏪

⏩

◀

▶

Back

Close

Full Screen / Esc

Printer-friendly Version

Interactive Discussion

shortage problem in the NCP has always been very serious since the new century and will be more severe as the economic development continues if no effective measures are taken in the future.

#### 4.5 Perspectives on sustainable water management

5 Groundwater pumping for agricultural irrigation, industrial and domestic use is also listed in Table 8. It shows that irrigation groundwater use accounts for about 79% of the total pumping over the simulation period (from 84% in 2000 to 76% in 2008). At the same time, the percentage of urban use groundwater relative to the total pumping water has increased from approximately 16% in 2000 to about 27% in 2007 (24% in 2008),  
10 which means that the industry has developed very quickly and required more water supplies during the simulation period. The industrial development and urbanization in the NCP aggravates the pressure of water supply as most cities' water supply mainly relies on groundwater. It is obvious that the more emphasis is placed on the economic development, the more water is required and the more pressure will be added to the sustainable development of water resources.

15 Considering that the water supply in the NCP is mainly groundwater, the protection of groundwater in this area appears especially important. Measures, such as importing surface water from outside river basins and using other sources of water than local groundwater, are effective groundwater protection possibilities. These measures will be greatly beneficial for mitigating the water shortage pressure in the NCP area. Another possibility is to choose measures that can reduce the evapotranspiration, such as changing the crop rotation type or adopting water-saving technologies that reduce evaporation. As shown in Table 8, agriculture is the largest water consumer in the NCP. Therefore it is a primary focus of water conservation attempts to improve the agricultural water use efficiency. Water saving irrigation techniques, such as border irrigation,  
20 low pressure pipe irrigation and sprinkler irrigation (Blanke et al., 2007), are the most effective measures that are used to replace the flood irrigation widely used in the NCP area.

**Integrated hydrological modeling of the North China Plain**

H. Qin et al.

Title Page

Abstract

Introduction

Conclusions

References

Tables

Figures



Back

Close

Full Screen / Esc

Printer-friendly Version

Interactive Discussion



Additional water allocated from the South-to-North Water Diversion Project (SNWDP) will play an important role in solving the water shortage problem in the NCP (Qin et al., 2012). The groundwater pumping for urban use and agricultural irrigation will be reduced once the SNWDP begins to work, as more surface water will be supplied for use. Other than water quantity protection, the protection of the water quality is also very important for the reason that water pollution will aggravate water shortage problem (Qin et al., 2012). The treated sewage can be reused in urban areas and for industry as water supply. Therefore, the wastewater reuse rate should be raised to help alleviate the water deficit of the NCP. A combination of reducing expenditure and controlled wastewater pollution has a dramatic impact on the sustainable water management. This aspect has been examined by Qin et al. (2012) and will be part of the future work of the NCP model.

## 5 Conclusions

An integrated and distributed hydrological model based on the coupled MIKE SHE/MIKE 11 code has been developed for the entire North China Plain. All major hydrological processes in the land phase of the hydrological cycle such as overland flow, rivers and lakes, unsaturated flow, evapotranspiration, and saturated flow as well as groundwater pumping and irrigation are included in the integrated hydrological model.

The model developed in this study is comprehensive and contains several innovative features. The pumping for domestic and industrial water use and the pumping for irrigation are estimated separately, where the domestic water consumption is approximated using a system dynamics model incorporating multiple sources of data (Qin et al., 2012). Since groundwater pumping accounts for a substantial fraction in the overall water balance, this improvement is considered significant. Another novel aspect of this study is the comparison of actual ET between model simulation and RS based estimates as a way of model validation. Moreover the hydrological model used in the present study is an integrated model including both surface water and

**HESSD**

10, 3693–3741, 2013

## Integrated hydrological modeling of the North China Plain

H. Qin et al.

[Title Page](#)

[Abstract](#)

[Introduction](#)

[Conclusions](#)

[References](#)

[Tables](#)

[Figures](#)

[⏪](#)

[⏩](#)

[◀](#)

[▶](#)

[Back](#)

[Close](#)

[Full Screen / Esc](#)

[Printer-friendly Version](#)

[Interactive Discussion](#)



## Integrated hydrological modeling of the North China Plain

H. Qin et al.

Title Page

Abstract

Introduction

Conclusions

References

Tables

Figures

⏪

⏩

◀

▶

Back

Close

Full Screen / Esc

Printer-friendly Version

Interactive Discussion



groundwater components while similar studies carried out in the same area only consider the groundwater component (Shu, 2010; Cao et al., 2013). The model is calibrated and validated against time series of hydraulic head data. It is known that the integrated hydrological models that are evaluated against groundwater head data alone often may not be able to provide reliable estimates beyond the scope of model calibration. However the potential strength of an integrated model as compared to a groundwater model such as the models developed by Jia and Liu (2002), Mao et al. (2005), Liu et al. (2008), Wang et al. (2008) and Cao et al. (2013) is that it is possible to use additional data sources than hydraulic head data to evaluate and/or constrain the model. We compare evapotranspiration with remote sensing based evapotranspiration data (Wu et al., 2012). The model is able to simulate the actual evapotranspiration in the right order of magnitude and with realistic temporal dynamics, suggesting that the water balance elements simulated by the model are reasonably accurate. Although the stream flow simulations are not able to be validated due to the lack of observational data, it is supposed not to have significant impact due to the small quantity. The results from the comparison of the model simulated ET and the remote sensing derived ET are very encouraging and there appears to be of good potential in using the ETWatch data to further constrain the model calibration. For example, Immerzeel and Droogers (2008) presented an innovative approach which incorporates remote sensing derived evapotranspiration in the calibration of the Soil and Water Assessment Tool (SWAT) in a catchment of the Krishna basin in southern India.

According to the model-calculated water balance, precipitation, evapotranspiration, irrigation and pumping are the major components controlling the hydrological system inflow and outflow of the NCP. The evapotranspiration is slightly larger than the precipitation, while the groundwater pumping takes up about 33 % of the precipitation and irrigation water in the NCP. Altogether, more outflows than inflows caused the aquifer storage to deplete continuously, which reveals unsustainable water resource development. About 79 % of the pumping water is used as the irrigation water, while the urban

use groundwater percentage of the total pumping has increased due to the economic development and population growth.

This model provides a powerful tool for evaluating the water resources in the NCP and particularly how changes in land use and agricultural management impact the groundwater resources. Sustainable water management is a key issue in the process of economic and social development of the NCP. The water balance analysis has significant implications for the sustainable water management in the NCP. Suggestions related to this issue include reducing evapotranspiration, the SNWDP, water saving irrigation techniques and water quality protection. These suggested approaches should be the focus of future studies based on the integrated model developed in this study. Evapotranspiration is the most important outflow component in the overall water balance, and is the only water actually consumed from the hydrologic system. Therefore, effective methods, such as changing crops to less consumptive water users and rain fed crops, fallowing land and urbanization, might be adopted to reduce ET. This will help greatly in mitigating the water deficit pressure and ensuring a sustainable water future for the NCP.

*Acknowledgements.* The support for this study is provided partially by a grant from China Geological Survey (#1212011121174). The co-authors from the three Danish organizations are supported by the grant from the Danish Strategic Research Council for the HYACINTS project under contract no: DSF-EnMi 2104-07-0008. We are grateful to Bingfang Wu at Chinese Academy of Sciences for providing the ET remote sensing data and Guiyu Yang at China Institute of Water Resources and Hydropower Research for providing the river network data. We also thank Sai Wang at Peking University for assistance with the manuscript preparation.

## HESSD

10, 3693–3741, 2013

### Integrated hydrological modeling of the North China Plain

H. Qin et al.

Title Page

Abstract

Introduction

Conclusions

References

Tables

Figures

⏪

⏩

◀

▶

Back

Close

Full Screen / Esc

Printer-friendly Version

Interactive Discussion



## References

- Abbott, M. B., Bathurst, J. C., Cunge, J. A., O'Connell, P. E., and Rasmussen, J.: An introduction to the European hydrological system-Systeme Hydrologique Europeen, SHE 1, history and philosophy of a physically based distributed modeling system, *J. Hydrol.*, 87, 45–59, 1986a.
- 5 Abbott, M. B., Bathurst, J. C., Cunge, J. A., O'Connell, P. E., and Rasmussen, J.: An introduction to the European Hydrological System-Systeme Hydrologique Europeen, SHE 1, structure of a physically based distributed modeling system, *J. Hydrol.*, 87, 61–77, 1986b.
- Anderson, M. P. and Woessner, W. W.: The role of the postaudit in model validation, *Adv. Water Resour.*, 15, 167–173, 1992.
- 10 Blanke, A., Rozelle, S., Lohmar, B., Wang, J., and Huang, J.: Water saving technology and saving water in China, *Agr. Water Manage.*, 87, 139–150, 2007.
- Braadbaart, O. and Braadbaart, F.: Policing the urban pumping race: industrial groundwater overexploitation in Indonesia, *World Dev.*, 25, 199–210, 1997.
- Branger, F., Braud, I., Debionne, S., Viallet, P., Dehotin, J., Henine, H., Nedelec, Y., and Anquetin, S.: Towards multi-scale integrated hydrological models using the LIQUID® framework: overview of the concepts and first application examples, *Environ. Modell. Softw.*, 25, 1672–1681, 2010.
- 15 Casper, M. C. and Vohland, M.: Validation of a large scale hydrological model with data fields retrieved from reflective and thermal optical remote sensing data – a case study for the Upper Rhine Valley, *Phys. Chem. Earth*, 33, 1061–1067, 2008.
- 20 Cao, G., Zheng, C., Scanlon, B. R., Liu, J., and Li, W.: Use of flow modeling to assess sustainability of groundwater resources in the North China Plain, *Water Resour. Res.*, 49, 1–17, doi:10.1029/2012WR011899, 2013.
- Cao, Z., Gareth, P., and Paul, C.: Shallow water hydrodynamic models for hyperconcentrated sediment-laden floods over erodible bed, *Adv. Water Resour.*, 29, 546–557, 2006.
- 25 Chen, J., Chen, X., Ju, W., and Geng, X.: Distributed hydrological model for mapping evapotranspiration using remote sensing inputs, *J. Hydrol.*, 305, 15–39, 2005.
- DHI: MIKE SHE User Manual, vol. 1: User Guide, Danish Hydraulic Institute, Horsholm, Denmark, 2008a.
- 30 DHI: MIKE SHE User Manual, vol. 2: Reference Guide, Danish Hydraulic Institute, Horsholm, Denmark, 2008b.

## Integrated hydrological modeling of the North China Plain

H. Qin et al.

Title Page

Abstract

Introduction

Conclusions

References

Tables

Figures

⏪

⏩

◀

▶

Back

Close

Full Screen / Esc

Printer-friendly Version

Interactive Discussion



## Integrated hydrological modeling of the North China Plain

H. Qin et al.

[Title Page](#)

[Abstract](#)

[Introduction](#)

[Conclusions](#)

[References](#)

[Tables](#)

[Figures](#)

[⏪](#)

[⏩](#)

[◀](#)

[▶](#)

[Back](#)

[Close](#)

[Full Screen / Esc](#)

[Printer-friendly Version](#)

[Interactive Discussion](#)



DHI: MIKE 11-A Modeling System for Rivers and Channels, Short Introduction and Tutorial, Danish Hydraulic Institute, Horsholm, Denmark, 2008c.

DHI: AUTOCAL-Auto Calibration Tool User Guide, Danish Hydraulic Institute, Horsholm, Denmark, 2008d.

5 Doummar, J., Sauter, M., and Geyer, T.: Simulation of flow processes in a large scale karst system with an integrated catchment model (Mike She) – identification of relevant parameters influencing spring discharge, *J. Hydrol.*, 426–427, 112–123, 2012.

Ferguson, I. M. and Maxwell, R. M.: Role of groundwater in watershed response and land surface feedbacks under climate change, *Water Resour. Res.*, 46, W00F02, doi:10.1029/2009WR008616, 2010.

10 Giovanni, P., Jonghan, K., Thomas, M., and Terry, H.: Determination of growth-stage-specific crop coefficients (Kc) of cotton and wheat, *Agr. Water Manage.*, 96, 1691–1697, 2009a.

Giovanni, P., Jonghan, K., Thomas, M., and Terry H.: Determination of growth-stage-specific crop coefficients (Kc) of maize and sorghum, *Agr. Water Manage.*, 96, 1698–1704, 2009b.

15 Goderniaux, P., Brouyère, S., Fowler, H. J., Blenkinsop, S., Therrien, R., Orban, P., and Das-sargues, A.: Large scale surface–subsurface hydrological model to assess climate change impacts on groundwater reserves, *J. Hydrol.*, 373, 122–138, 2009.

Henriksen, H. J., Trolborg, L., Nyegaard, P., Sonnenborg, T. O., Refsgaard, J. C., and Mad-sen, B.: Methodology for construction, calibration and validation of a national hydrological model for Denmark, *J. Hydrol.*, 280, 52–71, 2003.

20 Hoque, M. A., Hoque, M. M., and Ahmed, K. M.: Declining groundwater level and aquifer de-watering in Dhaka metropolitan area, Bangladesh: causes and quantification, *Hydrogeol. J.*, 15, 1523–1534, 2007.

Huai River Commission: *Hai He Gazetteer*, China Water & Power Press, Beijing, 1998.

25 Immerzeel, W. W. and Droogers, P.: Calibration of a distributed hydrological model based on satellite evapotranspiration, *J. Hydrol.*, 349, 411–424, 2008.

Jia, J. and Liu, C.: Groundwater regime and calculation of yield response in North China Plain: a case study of Luancheng County in Hebei Province, *J. Geogr. Sci.*, 12, 217–225, 2002.

30 Kang, L., Lei, Y., Zheng, L., Shu, Y., Zhang, Q., and Sun, S.: Vegetation classification based on MODIS data and the accuracy evaluation in the pixel scale, *Remote Sens. Technol. Appl.*, 22, 361–366, 2007.

## Integrated hydrological modeling of the North China Plain

H. Qin et al.

[Title Page](#)

[Abstract](#)

[Introduction](#)

[Conclusions](#)

[References](#)

[Tables](#)

[Figures](#)

[⏪](#)

[⏩](#)

[◀](#)

[▶](#)

[Back](#)

[Close](#)

[Full Screen / Esc](#)

[Printer-friendly Version](#)

[Interactive Discussion](#)

- Kendy, E., Gérard-Marchant, P., Walter, M. T., Zhang, Y., Liu, C., and Steenhuis, T. S.: A soil-water-balance approach to quantify groundwater recharge from irrigated cropland in the North China Plain, *Hydrol. Process.*, 17, 2011–2031, 2003.
- Kendy, E., Zhang, Y., Liu, C., Wang, J., and Steenhuis, T. S.: Groundwater recharge from irrigated cropland in the North China Plain: case study of Luancheng County, Hebei Province, 1949–2000, *Hydrol. Process.*, 18, 2289–2302, 2004.
- Kendy, E., Wang, J., Molden, D. J., Zheng, C., Liu, C., and Steenhuis, T. S.: Can urbanization solve inter-sector water conflicts? Insight from a case study in Hebei Province, North China Plain, *Water Policy*, 9, 75–93, 2007.
- Li, X., Zhang, Q., and Xu, C.: Suitability of the TRMM satellite rainfalls in driving a distributed hydrological model for water balance computations in Xinjiang catchment, Poyang lake basin, *J. Hydrol.*, 426–427, 28–38, 2012.
- Liu, C., Zhang, X., and Zhang, Y.: Determination of daily evaporation and evapotranspiration of winter wheat and maize by large-scale weighing lysimeter and microlysimeter, *Agr. Forest Meteorol.*, 111, 109–120, 2002.
- Liu, J., Zheng, C., Zheng, L., and Lei, Y.: Ground water sustainability: methodology and application to the North China Plain, *Ground Water*, 46, 897–909, 2008.
- Ma, L., Yang, Y., Yang, Y., Xiao, D., and Bi, S.: The distribution and driving factors of irrigation water requirements in the North China Plain, *J. Remote Sens.*, 15, 324–331, 2011.
- Madsen, H.: Parameter estimation in distributed hydrological catchment modeling using automatic calibration with multiple objectives, *Adv. Water Resour.*, 26, 205–216, 2003.
- Mao, X., Jia, J., Liu, C., and Hou, Z.: A simulation and prediction of agricultural irrigation on groundwater in well irrigation area of the piedmont of Mt. Thihang, North China, *Hydrol. Process.*, 19, 2071–2084, 2005.
- McMichael, C. E., Hope, A. S., and Loaiciga, H. A.: Distributed hydrological modelling in California semi-arid shrublands: MIKE SHE model calibration and uncertainty estimation, *J. Hydrol.*, 317, 307–324, 2006.
- Nash, J. E. and Sutcliffe, J. V.: River flow forecasting through conceptual models: Part 1: a discussion of principles, *J. Hydrol.*, 10, 282–290, 1970.
- National Bureau of Statistics of China: China Statistical Yearbook 2010, China Statistics Press, Beijing, China, 2010.
- Qin, H., Sun, A., Liu, J., and Zheng, C.: System dynamics analysis of water supply and demand in the North China Plain, *Water Policy*, 14, 214–231, 2012.

## Integrated hydrological modeling of the North China Plain

H. Qin et al.

Title Page

Abstract

Introduction

Conclusions

References

Tables

Figures

⏪

⏩

◀

▶

Back

Close

Full Screen / Esc

Printer-friendly Version

Interactive Discussion

- Rabus, B., Eineder, M., Roth, A., and Bamler, R.: The shuttle radar topography mission – a new class of digital elevation models acquired by spaceborne radar, *Isprs J. Photogramm.*, 57, 241–262, 2003.
- Refsgaard, J. C. and Storm, B.: MIKE SHE, in: *Computer Models of Watershed Hydrology*, edited by: Singh, V. P., Water Resources Publications, Littleton, chap. 23, 809–846, 1995.
- Shu, Y.: Integrating remote sensing and hydrological modeling for ground water resources assessment and sustainable use in the North China Plain, Ph.D. thesis, Department of Geography and Geology, Faculty of Science, University of Copenhagen, Denmark, 135 pp., 2010.
- Stisen, S., Jensen, K. H., Sandholt, I., and Grimes, D. I. F.: A remote sensing driven distributed hydrological model of the Senegal River basin, *J. Hydrol.*, 354, 131–148, 2008.
- Stisen, S., Højberg, A. L., Trolborg, L., Refsgaard, J. C., Christensen, B. S. B., Olsen, M., and Henriksen, H. J.: On the importance of appropriate precipitation gauge catch correction for hydrological modelling at mid to high latitudes, *Hydrol. Earth Syst. Sci.*, 16, 4157–4176, doi:10.5194/hess-16-4157-2012, 2012.
- van der Linden, S. and Woo, M.: Application of hydrological models with increasing complexity to subarctic catchments, *J. Hydrol.*, 270, 145–157, 2003.
- Wang, S., Shao, J., Song, X., Zhang, Y., Huo, Z., and Zhou, X.: Application of MODFLOW and geographic information system to groundwater flow simulation in North China Plain, China, *Environ. Geol.*, 55, 1449–1462, 2008.
- Wu, B., Xiong, J., and Yan, N.: ETWatch: An operational ET Monitoring System with Remote Sensing, The ISPRS workshop on Geo-Information and Decision Support Systems, Tehran, Iran, 6–7 January 2008a.
- Wu, B., Xiong, J., Yan, N., Yang, L., and Du, X.: ETWatch for monitoring regional evapotranspiration with remote sensing, *Adv. Water Sci.*, 19, 671–678, 2008b.
- Wu, B., Xiong, J., and Yan, N.: ETWatch: models and methods, *J. Remote Sens.*, 15, 224–239, 2011a.
- Wu, B., Xiong, J., and Yan, N.: ETWatch: calibration methods, *J. Remote Sens.*, 15, 240–254, 2011b.
- Wu, B., Yan, N., Xiong, J., Bastiaanssen, W. G. M., Zhu, W., and Stein, A.: Validation of ETWatch using field measurements at diverse landscapes: a case study in Hai Basin of China, *J. Hydrol.*, 436–437, 67–80, 2012.
- Wu, C., Xu, Q., Zhang, X., and Ma, Y.: Palaeochannels on the North China Plain: types and distributions, *Geomorphology*, 18, 5–14, 1996.

# HESSD

10, 3693–3741, 2013

## Integrated hydrological modeling of the North China Plain

H. Qin et al.

Title Page

Abstract

Introduction

Conclusions

References

Tables

Figures

⏪

⏩

◀

▶

Back

Close

Full Screen / Esc

Printer-friendly Version

Interactive Discussion



Xia, J., Zhang, L., Liu, C., and Yu, J.: Towards better water security in North China, *Water Resour. Manage.*, 21, 233–247, 2007.

Xiong, J., Wu, B., Yan, N., Zeng, Y., and Liu, S.: Estimation and validation of land surface evaporation using remote sensing and meteorological data in North China, *IEEE J. Sel. Top. Appl.*, 3, 337–344, 2010a.

Xiong, J., Wu, B., and Liu, S.: Estimation and calibration of remote sensed evapotranspiration for Hai river basin, in: *Haihe River Basins Research and Planning Approach*, Proceedings of 2009 International Symposium of Haihe Basin Integrated Water and Environment Management, edited by: Wen, W., Ling, J., Cheng, X., and Li, Y., Orient Academic Forum, Beijing, 200–214, 2010b.

Xu, Y., Mo, X., Cai, Y., and Li, X.: Analysis on groundwater table drawdown by land use and the quest for sustainable water use in the Hebei Plain in China, *Agr. Water Manage.*, 75, 38–53, 2005.

Yan, J. and Smith, K. R.: Simulation of integrated surface-water and ground-water systems-model formulation, *Water Resour. Bull.*, 30, 879–890, 1994.

Zhang, X., Pei, D., and Chen, S.: Root growth and soil water utilization of winter wheat in the North China Plain, *Hydrol. Process.*, 18, 2275–2287, 2004.

Zheng, C., Liu, J., Cao, G., Kendy, E., Wang, H., and Jia, Y.: Can China cope with its water crisis? Perspectives from the North China Plain, *Ground Water*, 48, 350–354, 2010.

Zektser, I. Z. and Everett, L. G.: *Groundwater resources of the world and their use*, IHP-VI, Series on Groundwater, N O.6, the United Nations Educational, Scientific and Cultural Organization (UNESCO), Paris, 2004.

Zhou, Y., Wang, L., Liu, J., Li, W., and Zheng, Y.: Options of sustainable groundwater development in Beijing Plain, China, *Phys. Chem. Earth*, 47–48, 99–113, 2012.

5  
10  
15  
20  
25

## Integrated hydrological modeling of the North China Plain

H. Qin et al.

[Title Page](#)

[Abstract](#)

[Introduction](#)

[Conclusions](#)

[References](#)

[Tables](#)

[Figures](#)

[⏪](#)

[⏩](#)

[◀](#)

[▶](#)

[Back](#)

[Close](#)

[Full Screen / Esc](#)

[Printer-friendly Version](#)

[Interactive Discussion](#)

**Table 1.** Sources of the data used in the coupled MIKE SHE/MIKE 11 hydrological model of the NCP.

Data name	Data type	Data sources
Topography	Distributed map	SRTM 90 m Digital Elevation Data ( <a href="http://srtm.csi.cgiar.org">http://srtm.csi.cgiar.org</a> )
Precipitation	Distributed map	TRMM 10 km Digital Precipitation Data ( <a href="http://trmm.gsfc.nasa.gov">http://trmm.gsfc.nasa.gov</a> )
Reference ET	Distributed map	Chinese Meteorological Data Service
Vegetation	Distributed map	MODIS NDVI based classification ( <a href="http://modis.gsfc.nasa.gov/data/">http://modis.gsfc.nasa.gov/data/</a> )
Leaf Area Index	Time series	Measured or from literature
Crop coefficient	Time series	Measured or from literature
Root depth	Time series	Measured or from literature
River network and cross sections	–	China Institute of Water Resources and Hydropower Research (IWHR)
River water levels and discharges	Time series	IWHR
Soil type	Distributed map	Soil map of Hebei province
Bottom elevation of each layer of the aquifer system	Distributed map	Geological map of North China Plain Geological Survey of China ( <a href="http://www.cgs.gov.cn">http://www.cgs.gov.cn</a> )
Geological units	Distributed map	Cao et al. (2012)
Observed wells	Time series	Cao et al. (2012)
Pumping wells	Time series	Qin et al. (2012)
Irrigation	Map	Shu et al. (2010)

## Integrated hydrological modeling of the North China Plain

H. Qin et al.

Title Page

Abstract

Introduction

Conclusions

References

Tables

Figures

⏪

⏩

◀

▶

Back

Close

Full Screen / Esc

Printer-friendly Version

Interactive Discussion

**Table 2.** Location and elevation information of the meteorological stations (Chinese Meteorological Data Service).

Station No.	Station Name	Municipality/Province	Elevation (m)	Latitude (°)	Longitude (°)
1	Anyang	Henan	62.9	36.05	114.40
2	Botou	Hebei	13.2	38.07	116.55
3	Baoding	Hebei	17.2	38.85	115.51
4	Huimin	Shandong	11.7	37.50	117.53
5	Tanggu	Tianjin	4.8	39.02	117.60
6	Shijiazhuang	Hebei	81.0	38.01	114.41
7	Raoyang	Hebei	19.0	38.23	115.73
8	Tai'an	Shandong	128.8	36.02	117.15
9	Zunhua	Hebei	54.9	40.11	117.58
10	Bazhou	Hebei	9.0	39.06	116.24
11	Xingtai	Hebei	77.3	37.01	114.50
12	Nangong	Hebei	27.4	37.37	115.40
13	Huanghua	Hebei	6.6	38.36	117.35
14	Jinan	Shandong	170.3	36.51	117.10
15	Weifang	Shandong	34.0	36.75	119.18
16	Luancheng	Hebei	50.1	37.90	114.65
17	Dongying	Shandong	6.0	37.46	118.49
18	Dezhou	Shandong	21.2	37.26	116.17
19	Heze	Shandong	49.7	35.25	115.43
20	Tianjin	Tianjin	2.5	39.08	117.07
21	Kaifeng	Henan	73.7	34.78	114.30
22	Zhengzhou	Henan	110.4	34.72	113.65

## Integrated hydrological modeling of the North China Plain

H. Qin et al.

**Table 3.** Typical values for LAI,  $K_c$  and root depth for different crops (Liu et al., 2002; Kendy et al., 2004; Zhang et al., 2004; Shu, 2010) and irrigation frequency and total irrigation water amount for these crops.

Crop type	$K_c$	LAI	Root depth (mm)	Irrigation frequency	Total irrigation water amount (mm)	
Winter wheat	10	0.3–1.1	0.5–6	800–2000	5	384
	20	0.3–1				
	30	0.3–1				
Summer corn	10	0.58–1	0.5–6	500–2000	2	115.2
	20	0.4–1.05				
	30	0.3–1.05				
Cotton	20	0–1.05	0.1–4.4	50–1200	2	78
	30	0–1.05				
Fruit tree		0.1–0.9	0.1–6	1000	5	254.4

Title Page

Abstract

Introduction

Conclusions

References

Tables

Figures

⏪

⏩

◀

▶

Back

Close

Full Screen / Esc

Printer-friendly Version

Interactive Discussion

## Integrated hydrological modeling of the North China Plain

H. Qin et al.

**Table 4.** Parameters for different soil types,  $\theta_{\text{sat}}$  is water content at saturation,  $\theta_{\text{fc}}$  is water content at field capacity,  $\theta_{\text{wp}}$  is water content as wilting point and  $K_{\text{s}}$  is saturated hydraulic conductivity.

Soil type	$\theta_{\text{sat}}$	$\theta_{\text{fc}}$	$\theta_{\text{wp}}$	$K_{\text{s}}(\text{ms}^{-1})$
Loam	0.46	0.35	0.13	$5.2 \times 10^{-6}$
Siltyloam	0.45	0.30	0.07	$1.3 \times 10^{-6}$
Sand	0.43	0.10	0.05	$1.0 \times 10^{-4}$

[Title Page](#)
[Abstract](#)
[Introduction](#)
[Conclusions](#)
[References](#)
[Tables](#)
[Figures](#)
[⏪](#)
[⏩](#)
[◀](#)
[▶](#)
[Back](#)
[Close](#)
[Full Screen / Esc](#)
[Printer-friendly Version](#)
[Interactive Discussion](#)

## Integrated hydrological modeling of the North China Plain

H. Qin et al.

Title Page

Abstract

Introduction

Conclusions

References

Tables

Figures

⏪

⏩

◀

▶

Back

Close

Full Screen / Esc

Printer-friendly Version

Interactive Discussion

**Table 5.** Information of the selected groundwater observation wells used in the calibration and validation processes (Cao et al., 2013). The information includes the location information and well elevation information that determines how deep the observed heads are measured in.

Well No.	Well Name	Municipality/ Province	Longitude (°)	Latitude (°)	Elevation (m)
6	Chaoyang	Beijing	116.51	40.02	200.00
35	Pinggu	Beijing	117.06	40.08	88.50
66	Shenze	Hebei	115.16	38.19	226.15
103	Daming	Hebei	115.33	36.33	30.84
116	Baoding	Hebei	115.51	38.85	96.00
123	Xiong	Hebei	116.17	38.96	253.50
129	Nanpi	Hebei	116.85	38.00	2.42
140	Yongqing	Hebei	116.54	39.34	256.75
214	Yanjin	Henan	114.34	35.32	30.00

## Integrated hydrological modeling of the North China Plain

H. Qin et al.

**Table 6.** Parameters selected for auto-calibration and the final values of them after the calibration process.  $K_i$  is horizontal conductivity for geological unit  $i$  ( $i$  is a positive integer),  $S_y(i)$  is storage coefficient for geological unit  $i$ .

Parameter	Initial value	Transformation	Parameter ties	Final value
$K_1(\text{ms}^{-1})$	$4.20 \times 10^{-5}$	Logarithmic		$3.97 \times 10^{-5}$
$S_{y1}$	0.07	Real		0.0866
$K_2(\text{ms}^{-1})$	$5.79 \times 10^{-5}$	Logarithmic	Tied to $K_1$	$3.97 \times 10^{-5}$
$K_3(\text{ms}^{-1})$	$1.157 \times 10^{-4}$	Logarithmic		$2.36 \times 10^{-4}$
$K_4(\text{ms}^{-1})$	$9.26 \times 10^{-5}$	Logarithmic		$7.79 \times 10^{-5}$
$S_{y4}$	0.07	Real	Tied to $S_{y1}$	0.0866
$K_5(\text{ms}^{-1})$	$8.68 \times 10^{-5}$	Logarithmic	Tied to $K_4$	$7.79 \times 10^{-5}$
$K_6(\text{ms}^{-1})$	$2.083 \times 10^{-4}$	Logarithmic	Tied to $K_3$	$2.36 \times 10^{-4}$
$K_7(\text{ms}^{-1})$	$3.472 \times 10^{-4}$	Logarithmic	Tied to $K_8$	$5.27 \times 10^{-4}$
$K_8(\text{ms}^{-1})$	$6.944 \times 10^{-4}$	Logarithmic		$5.27 \times 10^{-4}$
$S_{y10}$	0.15	Real		0.1360
$S_{y17}$	0.08	Real		0.0711
$S_{y23}$	0.0578	Real		0.0719

[Title Page](#)
[Abstract](#)
[Introduction](#)
[Conclusions](#)
[References](#)
[Tables](#)
[Figures](#)
[⏪](#)
[⏩](#)
[◀](#)
[▶](#)
[Back](#)
[Close](#)
[Full Screen / Esc](#)
[Printer-friendly Version](#)
[Interactive Discussion](#)

[Title Page](#)[Abstract](#)[Introduction](#)[Conclusions](#)[References](#)[Tables](#)[Figures](#)[⏪](#)[⏩](#)[◀](#)[▶](#)[Back](#)[Close](#)[Full Screen / Esc](#)[Printer-friendly Version](#)[Interactive Discussion](#)

**Table 7.** Performance results of the calibration and validation period. The summary result of the total 226 wells shown in Fig. 1 is also listed here. RMSE: root mean square error; ME: mean error; MAE: mean absolute error;  $STD_{res}$ : standard deviation of residuals;  $R$ : coefficient of correlation; and  $E$ : Nash–Sutcliffe model efficiency coefficient.

Target	RMSE (m)	ME (m)	MAE (m)	$STD_{res}$ (m)	$R$	$E$
Calibration period (2000–2005)						
Well#6	4.12	−0.08	3.16	4.12	0.91	0.34
Well#35	2.43	−1.41	1.89	1.98	0.68	0.14
Well#66	0.54	0.22	0.41	0.49	0.90	0.76
Well#103	1.32	1.01	1.11	0.86	0.75	−0.15
Well#116	2.50	−1.84	2.13	1.69	0.85	0.18
Well#123	2.71	−2.38	2.46	1.30	0.69	−2.35
Well#129	0.97	−0.74	0.80	0.63	0.79	0.10
Well#140	2.91	−0.60	2.62	2.85	0.56	−8.39
Well#214	1.02	−0.41	0.76	0.94	0.75	0.03
Validation period (2006–2008)						
Well#6	3.48	3.30	3.30	1.09	0.90	−0.96
Well#35	6.36	−6.09	6.09	1.83	0.95	−4.47
Well#66	0.45	−0.33	0.37	0.30	0.98	0.75
Well#103	1.08	−0.46	0.80	0.97	0.13	−0.69
Well#116	4.17	−4.10	4.10	0.78	0.36	−24.89
Well#123	1.18	−1.01	1.05	0.61	0.87	0.05
Well#129	0.44	0.14	0.37	0.42	0.46	−1.12
Well#140	5.71	5.48	5.48	1.58	0.56	−23.05
Well#214	0.71	0.24	0.60	0.66	0.82	0.63
Summary of the total observation wells						
	12.58	3.44	9.92	12.10	0.85	0.70

## Integrated hydrological modeling of the North China Plain

H. Qin et al.

**Table 8.** Annual water balance components (in unit mm) of the simulation period 2000–2008. ET: evapotranspiration; UZ: unsaturated zone; SZ: saturated zone.

Year Item	2000	2001	2002	2003	2004	2005	2006	2007	2008 (Jan–Aug)
Precipitation	574	421	377	734	609	563	468	550	472
Actual ET	582	574	538	524	585	584	537	558	433
Total irrigation	211	206	194	188	196	194	189	180	140
UZ storage change	–37	–46	–28	62	–17	–17	–18	24	13
SZ storage change	–23	–155	–178	97	–16	–63	–112	–98	–18
Groundwater recharge	242	100	62	337	239	193	141	150	167
Total pumping	251	248	238	236	248	249	249	246	184
Pumping for industrial and domestic use	40	42	44	48	52	55	60	66	44
Lateral inflow	3	5	7	6	5	5	6	7	5
Lateral outflow	15	10	9	8	9	8	7	7	4
Base flow to river	0.60	0.40	0.21	0.11	0.10	0.06	0.03	0.00	0.00
Base flow from river	0.21	0.19	0.16	0.13	0.13	0.11	0.11	0.09	0.06

Title Page

Abstract

Introduction

Conclusions

References

Tables

Figures

⏪

⏩

◀

▶

Back

Close

Full Screen / Esc

Printer-friendly Version

Interactive Discussion

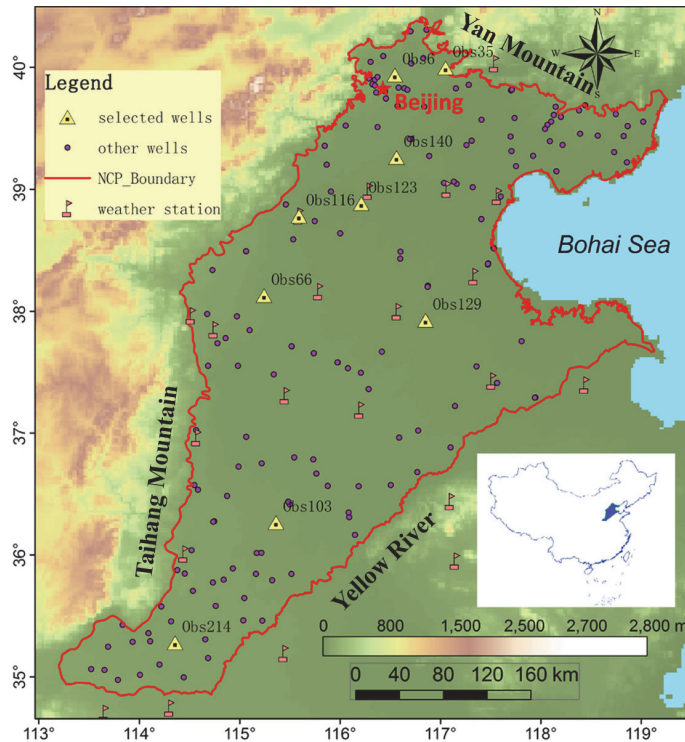
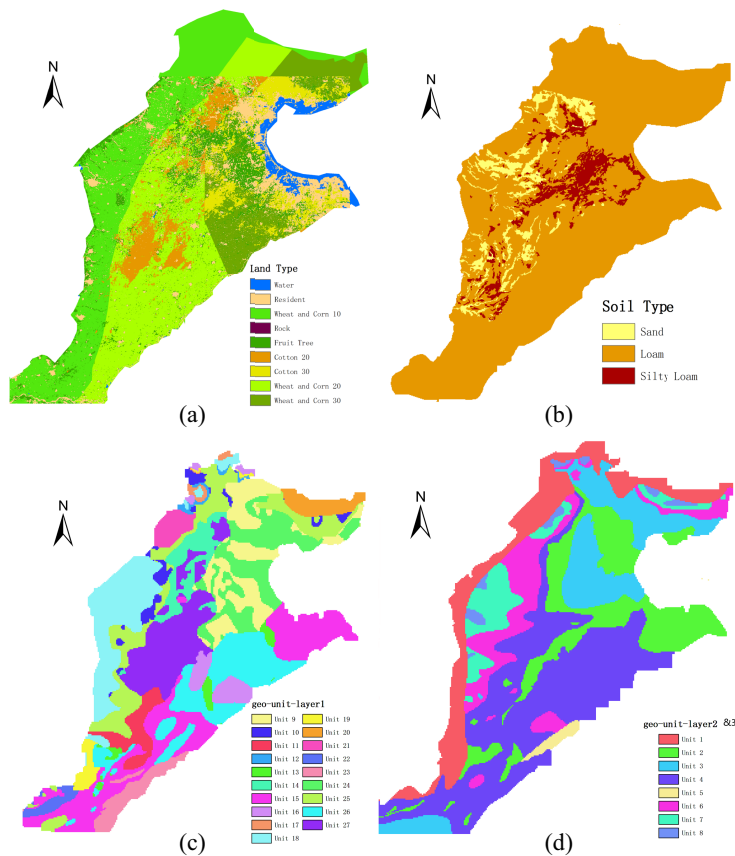


**Fig. 1.** Location and topography of the North China Plain, spanning from 32° N to 40° N and from 114° E to 121° E (Cao et al., 2013). Locations of meteorological stations and observation wells are also shown in the figure. The wells marked with rectangles are the selected wells used to show the calibration and validation results of groundwater heads.

Title Page	
Abstract	Introduction
Conclusions	References
Tables	Figures
◀	▶
◀	▶
Back	Close
Full Screen / Esc	
Printer-friendly Version	
Interactive Discussion	

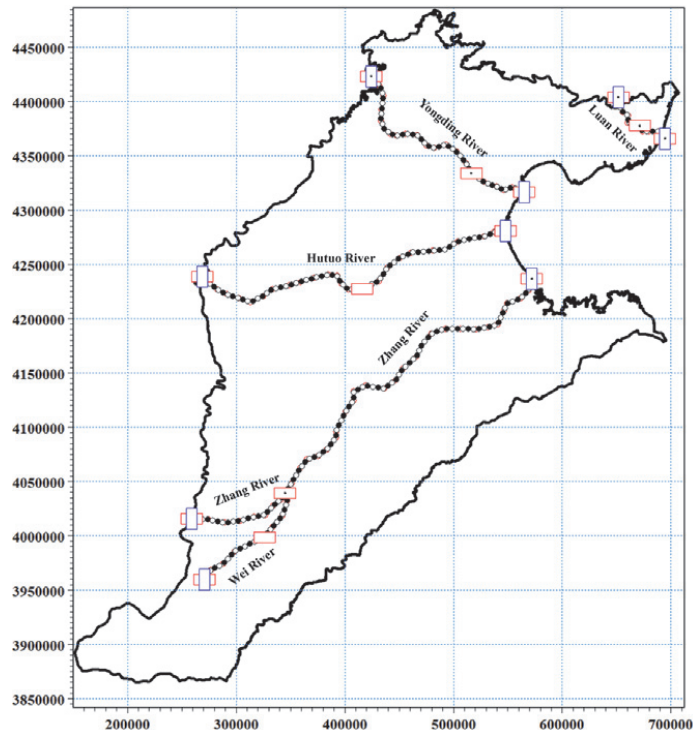
## Integrated hydrological modeling of the North China Plain

H. Qin et al.



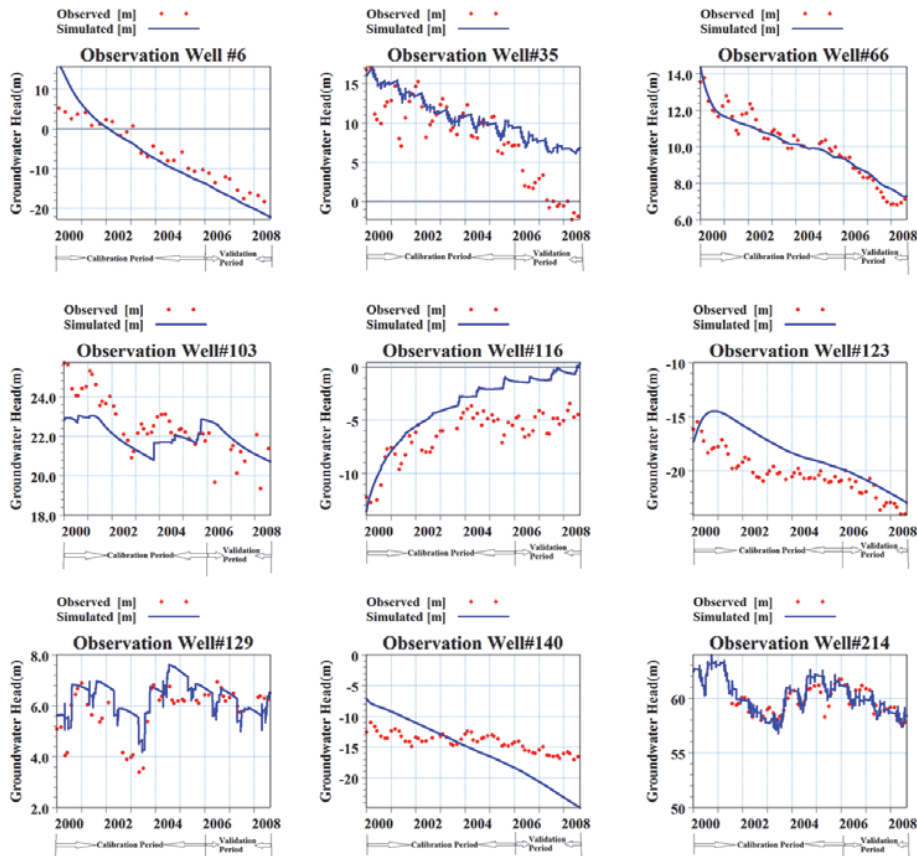
**Fig. 2.** (a) Land use types after Shu's model (2010); (b) soil types; (c) hydrogeological units of model layer 1 after the groundwater model of Cao et al. (2013); (d) hydrogeological units of model layers 2 and 3 after the groundwater model of Cao et al. (2013).

[Title Page](#)
[Abstract](#)
[Introduction](#)
[Conclusions](#)
[References](#)
[Tables](#)
[Figures](#)
[⏪](#)
[⏩](#)
[⏴](#)
[⏵](#)
[Back](#)
[Close](#)
[Full Screen / Esc](#)
[Printer-friendly Version](#)
[Interactive Discussion](#)



**Fig. 3.** River network of the NCP (IWR), including 5 major rivers: Luan River, Yongding River, Hutuo River, Zhang River and Wei River. The x- and y-axis represent the horizontal and vertical directions in unit of m.

[Title Page](#)[Abstract](#)[Introduction](#)[Conclusions](#)[References](#)[Tables](#)[Figures](#)[⏪](#)[⏩](#)[◀](#)[▶](#)[Back](#)[Close](#)[Full Screen / Esc](#)[Printer-friendly Version](#)[Interactive Discussion](#)

[Title Page](#)[Abstract](#)[Introduction](#)[Conclusions](#)[References](#)[Tables](#)[Figures](#)[⏪](#)[⏩](#)[◀](#)[▶](#)[Back](#)[Close](#)[Full Screen / Esc](#)[Printer-friendly Version](#)[Interactive Discussion](#)

**Fig. 4.** Comparison of simulated and observed groundwater heads for selected observation wells distributed in the North China Plain. The calibration period is 2000–2005 while the validation period is 2006–2008.

## Integrated hydrological modeling of the North China Plain

H. Qin et al.

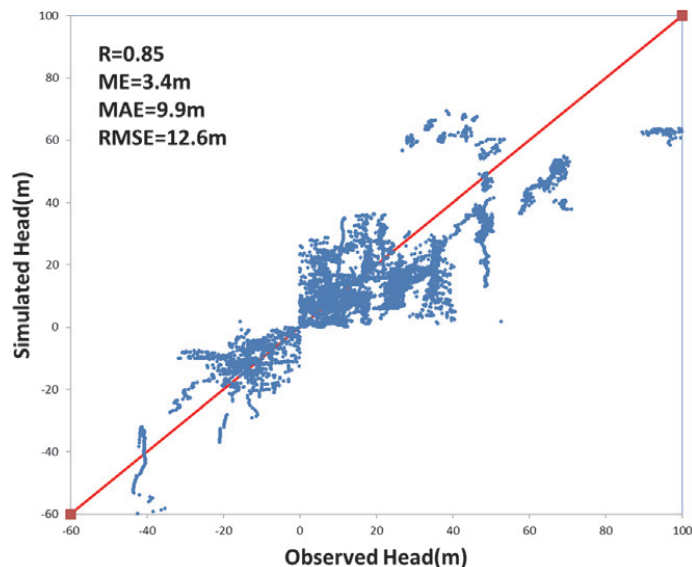


**Fig. 5.** Scatter plot of simulated and observed groundwater heads for the entire 226 observation wells. The points that lack observed head data have been rejected from the figure. The performance criteria values ( $R$ ,  $ME$ ,  $MAE$  and  $RMSE$ ) are also shown in the figure.

[Title Page](#)[Abstract](#)[Introduction](#)[Conclusions](#)[References](#)[Tables](#)[Figures](#)[⏪](#)[⏩](#)[◀](#)[▶](#)[Back](#)[Close](#)[Full Screen / Esc](#)[Printer-friendly Version](#)[Interactive Discussion](#)

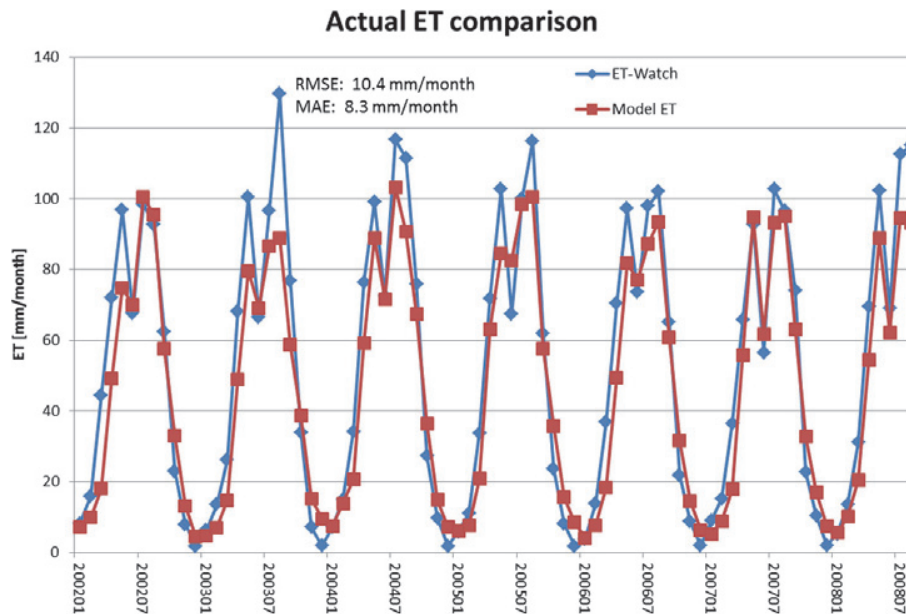


**Fig. 6.** Monthly comparison of aggregated mean ET values for the entire model domain. RMSE and MAE values given are based on linear regression analysis.

[Title Page](#)[Abstract](#)[Introduction](#)[Conclusions](#)[References](#)[Tables](#)[Figures](#)[⏪](#)[⏩](#)[◀](#)[▶](#)[Back](#)[Close](#)[Full Screen / Esc](#)[Printer-friendly Version](#)[Interactive Discussion](#)

## Integrated hydrological modeling of the North China Plain

H. Qin et al.

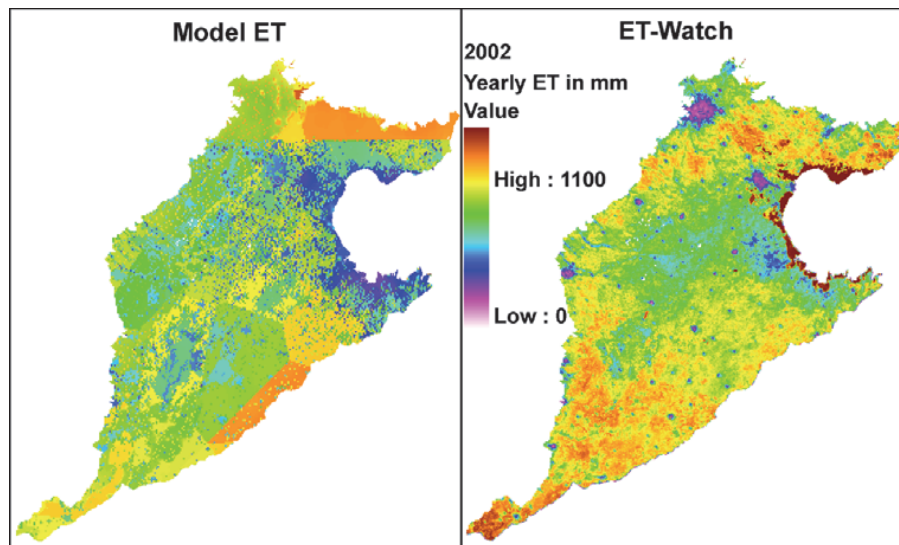


**Fig. 7.** Annually aggregated ET from the model and from ET-Watch. The spatial resolution of the model ET is 2 km while it is 1 km for the ET-Watch data. The same color scale is applied to the two datasets. Only part of the model domain covered by both products have been considered, which mainly excludes some areas along the south-eastern part of the model domain.

[Title Page](#)[Abstract](#)[Introduction](#)[Conclusions](#)[References](#)[Tables](#)[Figures](#)[⏪](#)[⏩](#)[◀](#)[▶](#)[Back](#)[Close](#)[Full Screen / Esc](#)[Printer-friendly Version](#)[Interactive Discussion](#)

## Integrated hydrological modeling of the North China Plain

H. Qin et al.

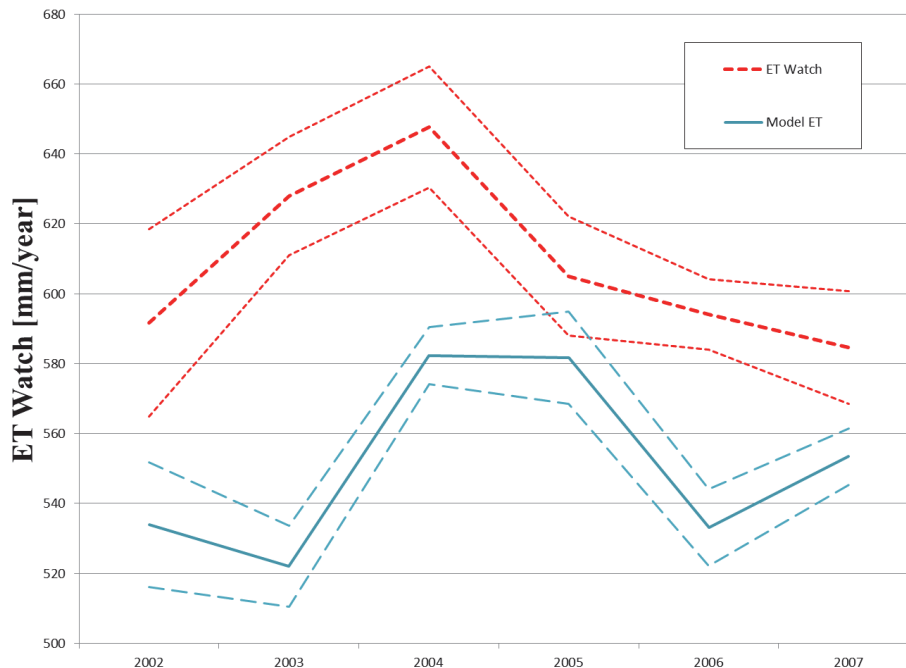


**Fig. 8.** Annual mean ET from the model simulation (bold blue line) and the ET-watch (bold red line). The lighter lines represent  $\pm$  one standard deviation from the mean values for each of the eight land cover classes considered.

[Title Page](#)[Abstract](#)[Introduction](#)[Conclusions](#)[References](#)[Tables](#)[Figures](#)[⏪](#)[⏩](#)[⏴](#)[⏵](#)[Back](#)[Close](#)[Full Screen / Esc](#)[Printer-friendly Version](#)[Interactive Discussion](#)

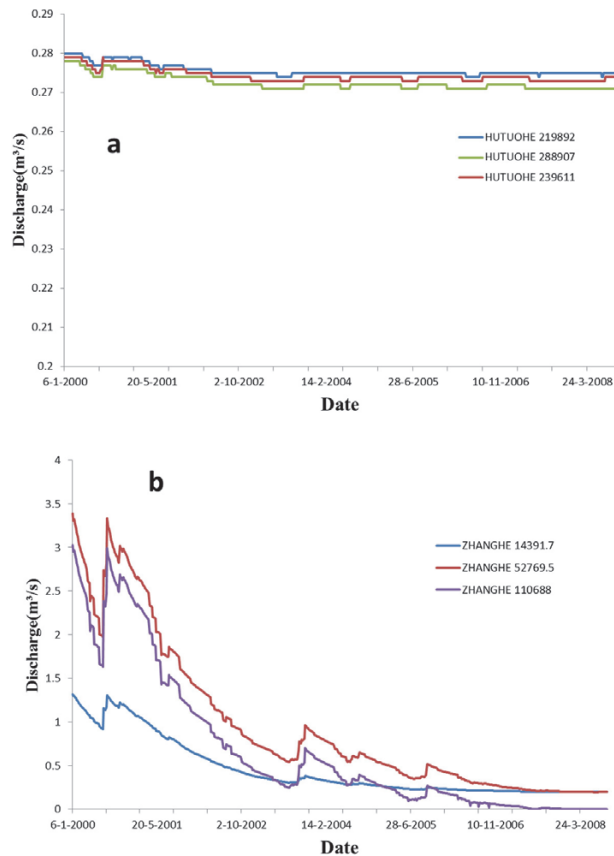


**Fig. 9.** Simulated discharge at three locations along (a) Hutuo River and (b) Zhang River. The number behind the river name represents the chainage of that location.

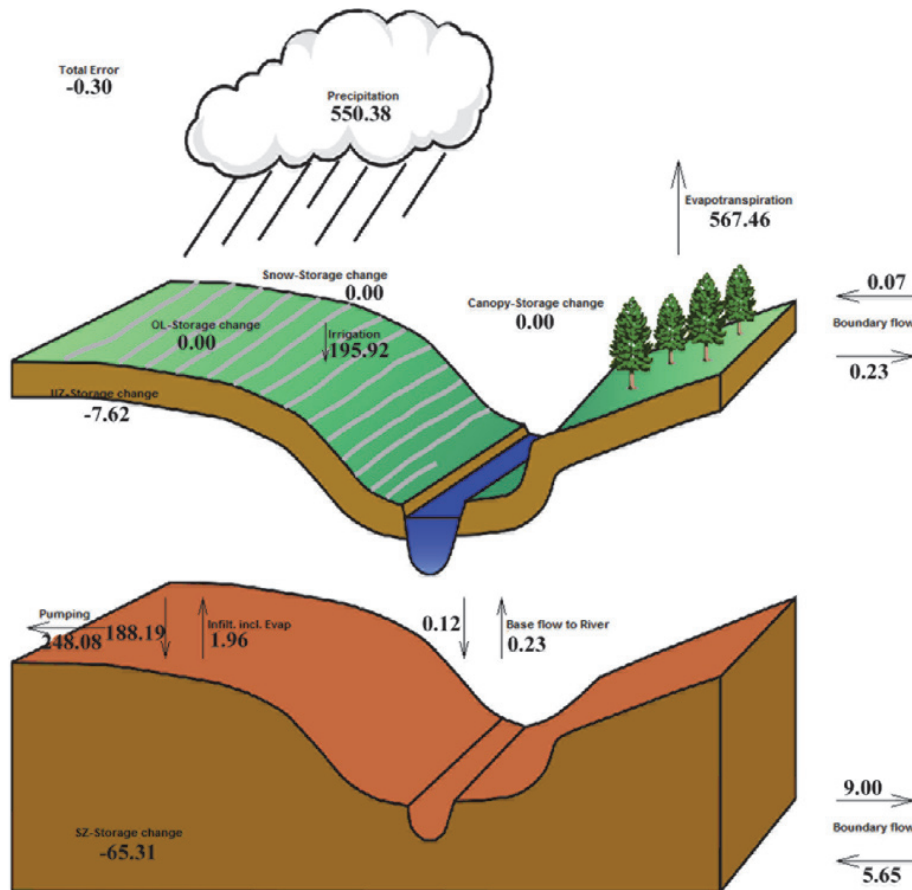


**Fig. 10.** Graphical water balance result of the entire NCP aquifer system. The numbers in the figure are normalized annual averaged values in the type of storage depth with unit of  $\text{mm yr}^{-1}$ .

[Title Page](#)  
[Abstract](#)   [Introduction](#)  
[Conclusions](#)   [References](#)  
[Tables](#)   [Figures](#)  
[◀](#)   [▶](#)  
[◀](#)   [▶](#)  
[Back](#)   [Close](#)  
[Full Screen / Esc](#)  
[Printer-friendly Version](#)  
[Interactive Discussion](#)

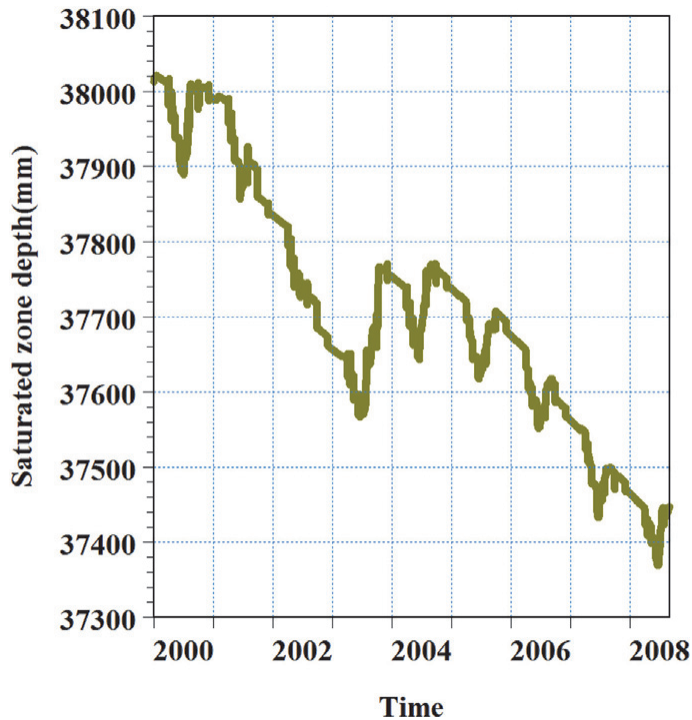


Fig. 11. Saturated zone storage depth over time of the study area from 2000 to 2008.

# HESSD

10, 3693–3741, 2013

## Integrated hydrological modeling of the North China Plain

H. Qin et al.

[Title Page](#)

[Abstract](#) | [Introduction](#)

[Conclusions](#) | [References](#)

[Tables](#) | [Figures](#)

[◀](#) | [▶](#)

[◀](#) | [▶](#)

[Back](#) | [Close](#)

[Full Screen / Esc](#)

[Printer-friendly Version](#)

[Interactive Discussion](#)



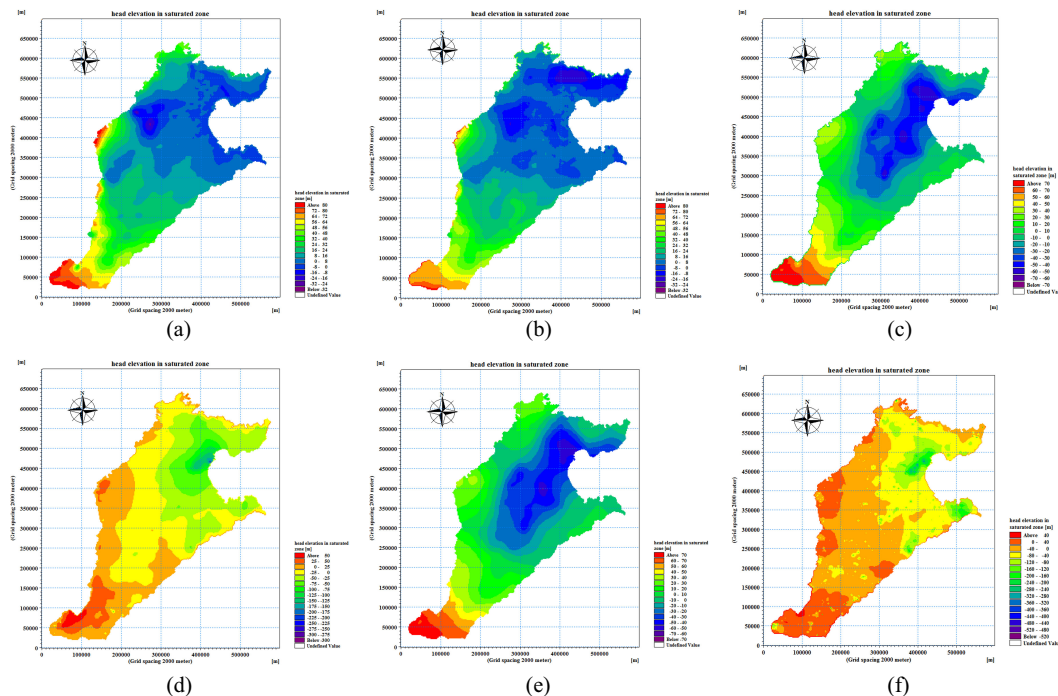


**Fig. 12.** Simulated groundwater head configurations on 1 January 2000 and 31 August 2008. (a), (c) and (e) are head elevations on 1 January 2000 for layer 1, 2, and 3, respectively; (b), (d) and (f) are head elevations on 31 August 2008 for layer 1, 2, and 3, respectively.

Title Page

Abstract

Introduction

Conclusions

References

Tables

Figures

⏪

⏩

⏴

⏵

Back

Close

Full Screen / Esc

Printer-friendly Version

Interactive Discussion